

SZ Lyncis: A Non-Accreting Neutron Star- δ Scuti Binary Candidate Discovered via Dynamics and Asteroseismology

PING LI,^{1,2} LI-YING ZHU,^{1,2} AND WEN-PING LIAO^{1,2}

¹*Yunnan Observatories, Chinese Academy of Sciences (CAS), 650216 Kunming, P.R. China*

²*University of Chinese Academy of Sciences, No.1 Yanqihu East Rd, Huairou District, Beijing, P.R.China 101408*

ABSTRACT

Neutron stars (NSs) are traditionally discovered through radio, X-ray, or gamma-ray observations, but optical time-domain surveys can unveil non-accreting NSs in wide binaries. Here we report a NS candidate in the single-lined binary SZ Lyncis, identified through a combination of asteroseismology, spectroscopy, pulsation timing, and astrometry. The visible δ Scuti primary has a mass of $M_1 = 1.83_{-0.01}^{+0.06} M_\odot$ from asteroseismic modeling. With the orbital inclination ($i = 38.67 \pm 0.29^\circ$) from the astrometric data of Gaia and Hipparcos, we obtain companion masses of $M_2 = 1.76_{-0.042}^{+0.042} M_\odot$ (radial velocity) and $M_2 = 2.07_{-0.045}^{+0.045} M_\odot$ (timing variations). The companion's mass exceeds the Chandrasekhar limit and lies in the NS range. Multiple arguments rule out alternatives: the astrometric mass function and the spectral energy distribution, which shows no extra light, together exclude any luminous companion; the mass and lack of Balmer absorption rule out white dwarfs (WDs); the system's age (1.25 Gyr) disfavors a double WD; and the mass is too low for a black hole. The wide, low-eccentricity orbit and absence of accretion signatures are consistent with a quiescent NS. SZ Lyn has the potential to be the first δ Scuti binary with a NS candidate identified through asteroseismology and dynamics, demonstrating the potential of this approach to uncover non-accreting compact objects.

Keywords: Delta Scuti variable stars (370) — Asteroseismology(73) — Neutron stars(1108)

1. INTRODUCTION

The mass distribution and physical properties of neutron stars (NSs) encode crucial information about stellar evolution history and Galactic chemical enrichment (Özel et al. 2012; Yi et al. 2022). While typically detected through electromagnetic emission – including rapidly rotating, highly magnetized radio pulsars (Lorimer 2008), accreting X-ray binaries, gamma-ray pulsars (Abdo et al. 2010), and isolated thermally emitting NSs (Haberl 2007) – with merging NS systems additionally detectable via LIGO/Virgo gravitational-wave observatories (Abbott et al. 2017), these methods possess inherent limitations. Radio, X-ray, and gamma-ray detection requires either favorable beaming geometry or ongoing accretion processes (Yi et al. 2022), leaving non-accreting and radio-quiet NS populations largely undetected (Caraveo et al. 1996).

δ Scuti variable stars (A–F spectral types) occupy the main-sequence region intersecting the classical Cepheid instability strip in the Hertzsprung–Russell diagram. Their oscillations, driven by the κ mechanism in the He II partial ionization zone, produce stable periodic signals with periods of 15 minutes to 8 hours (Aerts et al. 2010; Breger et al. 1993). High-amplitude δ Scuti stars (HADS)—defined by photometric variations ≥ 0.1 mag and typically slow rotation ($v \sin i \leq 30 \text{ km s}^{-1}$)—function as exceptional celestial chronometers (Niu et al. 2026). Their remarkable pulsational stability enables precise detection of minuscule period variations induced by orbital motion through the light-travel time effect (LTTE) (Irwin 1952).

SZ Lyncis (SZ Lyn; TIC 192939152) is a well-studied HADS in a single-line spectroscopic binary system, with a mean magnitude of $\langle V \rangle = 9.1$ mag where only the brighter component (SZ Lyn A) is spectroscopically observable while the fainter companion (SZ Lyn B) remains undetected (Gazeas et al. 2004; Bardin & Imbert 1981). The fundamental

pulsation period was first established by Binnendijk (1968) and subsequently refined by Gazeas et al. (2004), with orbital studies showing that the linear ephemeris for pulsation maxima is modulated by long-term orbital motion through the LTTE (Barnes & Moffett 1975). Both pulsation and orbital parameters have been progressively improved through later analyses (Moffett et al. 1988; Paparo et al. 1988; Li & Qian 2013; Gazeas et al. 2004). Recently, Adassuriya et al. (2021) identified in SZ Lyn A a dominant radial mode ($f_1 = 8.296 \text{ d}^{-1}$), two non-radial p-modes ($f_2 = 14.535 \text{ d}^{-1}$, $f_3 = 32.620 \text{ d}^{-1}$), and a potential g-mode ($f_4 = 4.584 \text{ d}^{-1}$). The physical parameters of SZ Lyn A determined by previous authors and our work are summarized in Table 1, though the mass and radius of SZ Lyn A have not been accurately determined in earlier studies.

Table 1. Physical parameters of SZ Lyn A.

Parameter	Value	Reference
T_{eff} (K)	7173	LAMOST (this paper)
	7799	<i>Gaia</i>
	6750	Adassuriya et al. (2024)
$\log(g)$	3.50	Adassuriya et al. (2024)
	3.87	LAMOST (this paper)
Mass (M_{\odot})	$1.57^{+0.17}_{-0.66}$	Fernley et al. (1984)
	1.7-2.0	Adassuriya et al. (2021)
Radius (R_{\odot})	$2.76^{+0.11}_{-0.46}$	Fernley et al. (1984)
	2.80	Bardin & Imbert (1981)
Parallax (mas)	2.49 ± 0.07	<i>Gaia</i>

Two key developments now enable a definitive reassessment of this system. First, high-precision, continuous photometry from the Transiting Exoplanet Survey Satellite (TESS) (Ricker et al. 2015) provides exquisite characterization of the primary star’s pulsation modes, yielding significantly improved determinations of mass and radius for SZ Lyn A along with precise times of maximum light. Second, by incorporating the orbital inclination derived from Hipparcos and Gaia data, we can estimate the mass of SZ Lyn B through dynamical analysis combining radial velocity (RV) measurements and the LTTE, and determine its nature.

Building on these advances, our comprehensive analysis combines TESS photometry with times of maximum light and RV measurements to reveal an astrophysical treasure: a wide, low-eccentricity orbit harboring a compact companion. Mass estimates of $M_2 = 1.76^{+0.042}_{-0.042} M_{\odot}$ (RV method) and $M_2 = 2.07^{+0.045}_{-0.045} M_{\odot}$ (LTTE method) indicate that SZ Lyn B is a NS. If this is correct, it would be the first NS known to orbit a δ Scuti star at a distance of 397 pc.

The system exhibits notable characteristics: it ranks among the rare binaries hosting both a main-sequence pulsator and a NS candidate, enabling potential asteroseismology in strong gravity; its wide, low-eccentricity orbit offers constraints for supernova kick models; and it pioneers the synergy of asteroseismology with dynamical methods (radial velocity and LTTE) for compact companion detection. Collectively, these features indicate SZ Lyn may represent a scientifically valuable system, with potential implications for understanding stellar evolution and advancing compact star searches.

2. RESULTS AND DISCUSSION

2.1. Asteroseismic properties of SZ lyn A

Analysis of the TESS photometry confirms SZ Lyn A as a multi-periodic pulsator, revealing six significant frequencies including four previously reported by Adassuriya et al. (2021). To provide complementary constraints on the system properties, we conducted asteroseismic modeling of the primary star. Using Modules for Experiments in Stellar Astrophysics (MESA) (Paxton et al. 2011, 2013, 2015, 2018), we computed a grid of stellar evolutionary models, then derived their adiabatic pulsation frequencies with *pulse_adipls* (Christensen-Dalsgaard 2008). The optimal model, selected through frequency matching of all six observed pulsation modes following the identification framework of Adassuriya et al. (2021), is presented in Table 5 (In Appendix).

The best-fit model (Table 4 in Appendix) places SZ Lyn A on the post-main sequence, yielding the following parameters: mass $M = 1.83_{-0.01}^{+0.06} M_{\odot}$, effective temperature $T_{\text{eff}} = 6791_{-58}^{+51}$ K, radius $R = 2.899_{-0.000}^{+0.027} R_{\odot}$, luminosity $L = 16.111_{-0.354}^{+0.721} L_{\odot}$, and age $= 1.254_{-0.024}^{+0.079}$ Gyr. Notably, the derived mass and radius are consistent with the values in Table 1 but exhibit significantly reduced uncertainties.

2.2. The orbital ephemeris, radial velocity curve, and the mass function

The orbital ephemeris of SZ Lyn A is:

$$T(\phi = 0) = 2445156.600(\text{HJD}) + 1181^d.5(1.4) \times N \quad (1)$$

where the first term is the primary eclipse time (denoted as T_0), and the second term is the orbital period in day times the number of orbital cycles N (Bardin & Imbert 1984), HJD is the Heliocentric Julian Date.

As shown in Figure 1, a low-resolution spectrum of SZ Lyn was taken from DR7 of LAMOST low-resolution single-epoch spectra. The University of Lyon Spectroscopic Analysis Software (ULySS) (Koleva et al. 2009) was used to obtain stellar atmospheric parameters: $T_{\text{eff}}=7173 (\pm 146)$ K, $\log g=3.87 (\pm 0.01)$, $[Fe/H]=-0.08 (\pm 0.01)$. The cross-corresponding function (CCF) method is used to obtain a RV value (32 ± 4 km/s). We also collected 21 RV values from Bardin & Imbert (1984), covering one orbital period of SZ Lyn. According to Equation (1), The RV data are phase-folded.

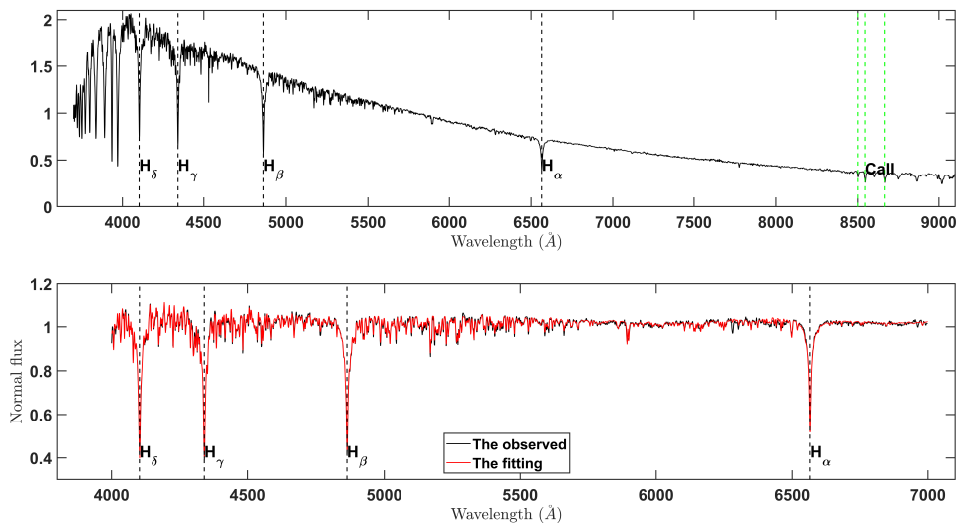


Figure 1. The low-resolution spectrum of SZ Lyn observed with LAMOST. Upper panel: The original spectrum, the four Balmer absorbed lines H_{α} , H_{β} , H_{γ} , and H_{δ} and the metal lines CaII are marked. Lower panel: The fitting model of A-type star for the spectrum of SZ Lyn.

The following equations (Iglesias-Marzoa et al. 2015) are used to fit the RV values

$$V_r = \gamma + K[\cos(\theta + \omega) + e \cos(\omega)], \quad (2)$$

$$\theta(t) = 2 \arctan\left[\sqrt{\frac{1+e}{1-e}} \tan\left(\frac{E}{2}\right)\right], \quad (3)$$

$$E - e \sin(E) = \frac{2\pi}{P}(t - T_p), \quad (4)$$

where γ , K , ω , e , E , P , and T_p are the center of mass velocity of binary system, the semi-amplitude of RV, the eccentricity of the orbit, the eccentric anomaly, the orbital period of binary system. and the time of periastron passage, respectively.

Figure 2 shows that the fitting results of RV in $\gamma=34.18 (\pm 0.05)$ (km/s), $K=9.51 (\pm 0.09)$ (km/s), $\omega=101.2 (\pm 1.4)^\circ$, $e=0.186 (\pm 0.009)$, $P=1188.51 (\pm 7.59)$ days and $T_p=2452751.81 (\pm 19.13)$, respectively. Hence the mass function (lower mass limit) for SZ Lyn B is:

$$f(M_2) = \frac{(M_2 \sin i)^3}{(M_1 + M_2)^2} = \frac{PK^3}{2\pi G} (1 - e^2)^{3/2} = 0.1031 \pm 0.0030 M_\odot \quad (5)$$

where M_1 and M_2 are the masses of SZ Lyn A and B, respectively, i is the orbital inclination, and G is the gravitational constant.

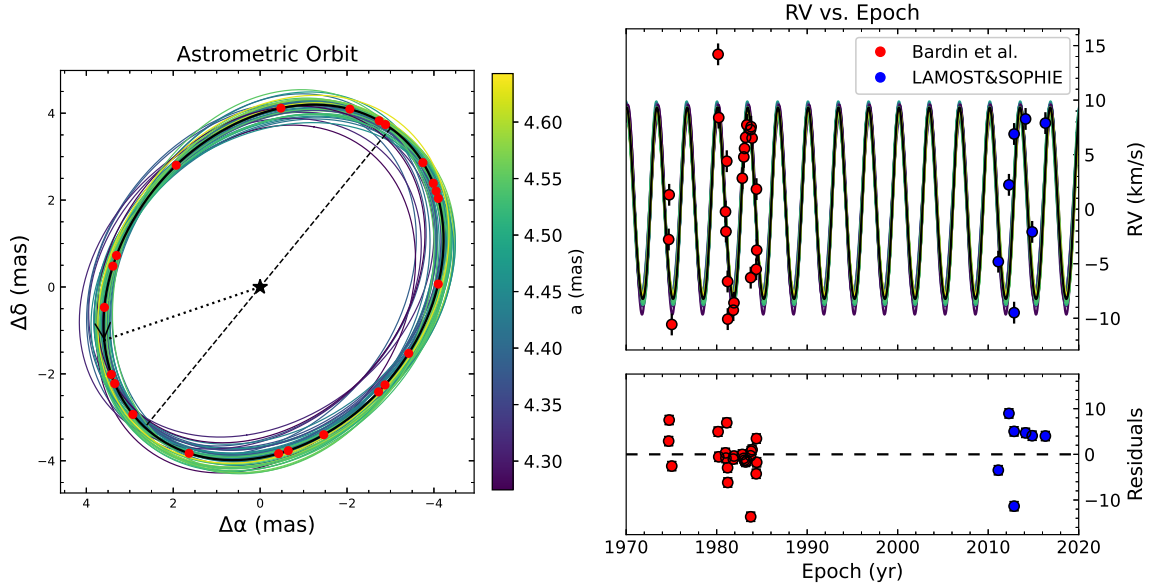


Figure 2. Left panel: predicted observation times of SZ Lyn from the Gaia Observation Scheduling Tool (GOST) and Hipparcos HIP1 and 2. The black line shows the best-fitting orbit using the orvara code from our combined fit to the radial velocity data, Hipparcos astrometry, and the GOST scan time predictions. The red points show the model-predicted photocentre positions at the times when GOST predicts Gaia would have observed the source, computed from the best-fitting orbit. We do not have access to the actual measured Gaia astrometric positions (RA, Dec); only to the predicted scan times. The expected per-epoch astrometric uncertainties are approximately 0.2 mas in the along-scan direction. The predicted scan times demonstrate that the orbit has been sampled adequately. Right panel: the radial velocity curve of SZ Lyn.

2.3. The $O-C$ analysis (LTTE) of the pulsation maximum

The orbital ephemeris of SZ Lyn is:

$$T' = 2438124.39955(HJD) + 0^d.12053491 \times E \quad (6)$$

where the first term is the pulsation maximum time (denoted as T'_0), and the second term is the pulsation period in day times the number of pulsation cycles E (Paparo et al. 1988).

We obtained 413 pulsation maximum from the light curves observed by TESS. There are 202 pulsation maximum are collected from Adassuriya (2022), observed by AAVSO, WASP (Wide Angle Search for Planets) and Abu (Adassuriya et al. 2021). In addition, we also collected 337 pulsation maximum from Agerer & Hubscher (2003); Derekas et al. (2003); Gazeas et al. (2004); Agerer & Hubscher (2003); Klingenberg et al. (2006); Samolyk (2010, 2011, 2012, 2013); Hubscher & Walter (2007); Hubscher et al. (2006, 2009a); Hubscher & Lehmann (2012); Hubscher et al. (2010, 2009b, 2005, 2013); Wils et al. (2013). According to Equation 6, pulsation maximum data are converted to $O - C$ and pulsation number cycles. The following equations (Irwin 1952) are used to fit the $O - C$ values

$$O - C = \Delta T_0 + \Delta P_0 \cdot E + A \left[\sqrt{1 - e^2} \sin E^* \cos \omega + \cos E^* \sin \omega \right], \quad (7)$$

and the Kepler's equation:

$$M = E^* - e \sin E^* = \frac{2\pi(t - T)}{P} \quad (8)$$

where ΔT_0 and ΔP_0 denote the revised epoch and period, A is the $O-C$ semi-amplitude, e the eccentricity, ν the true anomaly, ω the longitude of periastron, M the mean anomaly, T the periastron passage time, t the observed pulsating maximum times, P the orbital period, and E^* the eccentric anomaly.

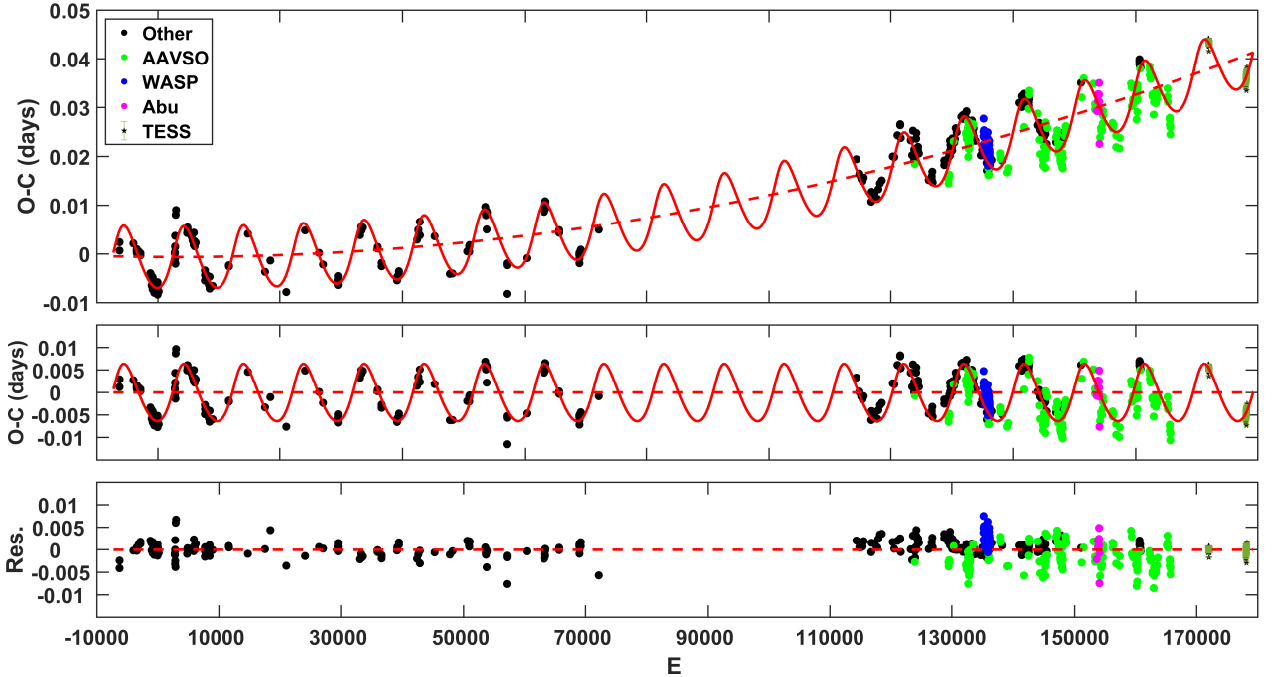


Figure 3. The radial $O - C$ curve of SZ lyn.

We used LTTE model to fit the $O - C$ data using the MCMC method. Figure 3 shows that the fitting results in $A=0.00651(\pm 0.00005)$ d, $P'=3.24170(\pm 0.00075)$ yr, where A and P' are the semi-amplitude and period of $O - C$. Therefore the mass function (lower mass limit) for SZ Lyn B is:

$$f(M_2) = \frac{(M_2 \sin i)^3}{(M_1 + M_2)^2} = \frac{4\pi^2}{GP'^2} (a_{12} \sin i)^3 = 0.1365 \pm 0.0031 M_\odot \quad (9)$$

where $a_{12} \sin i = A \times c$ (c is the speed of light) is the project semi axis.

2.4. Unveiling the nature of SZ Lyn B

The orbital inclination of SZ Lyn has been determined to be $i = 38.67 \pm 0.29^\circ$ (Figure 2) using astrometric data from Gaia, which is close to the previous value of $i = 39.6 \pm 17.7^\circ$ obtained using Hipparcos astrometric data (see (Li & Qian 2013)). Using Equations 5 and 9, the mass of SZ Lyn B derived from radial velocity measurements is $M_2 = 1.76^{+0.042}_{-0.042} M_\odot$, while $O-C$ analysis yields $M_2 = 2.07^{+0.045}_{-0.045} M_\odot$; these results are consistent within uncertainties. The corresponding orbital separations are $a_{RV} = 3.342^{+0.046}_{-0.046}$ astronomical units (au) and $a_{O-C} = 3.449^{+0.035}_{-0.035}$ au, respectively.

Multiple lines of evidence argue against SZ Lyn B being a luminous companion, whether a single star or a close main-sequence binary. If the companion contributes any light (Figure 5), its astrometrically inferred mass increases. The dotted cyan line shows the expected flux ratio and mass for a single main-sequence companion, which always lies below the black line, ruling out any single main-sequence companion as the explanation for the observed orbit. The same holds for an equal-mass inner binary (yellow dashed). Even an inner binary composed of a $1.0 M_\odot$ WD and

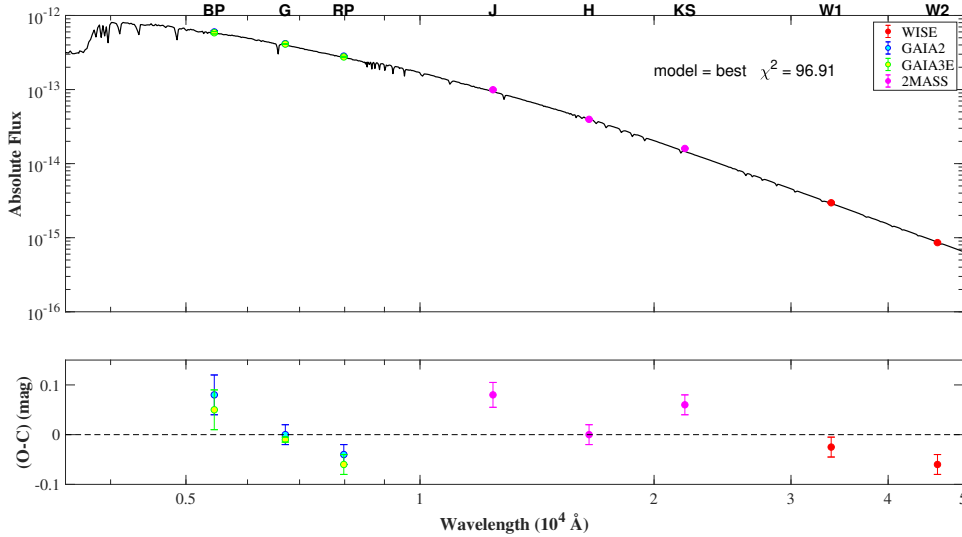


Figure 4. The broad band spectral-energy distribution of SZ Lyn.

a main-sequence star (blue dashed) has a mass-to-light ratio too low to match the astrometric mass function. This conclusion is further supported by: (1) the absence of spectral lines moving in antiphase to SZ Lyn A in both our low-resolution spectra and the high-resolution data of [Adassuriya et al. \(2024\)](#); (2) the $O-C$ diagram of pulsation maxima (Figure 3) showing only a single variation component; and (3) the spectral energy distribution (SED) (Figure 4) being well fitted by an A-type star model at both blue and red ends, with no excess indicative of an additional luminous component. Therefore, SZ Lyn B is unlikely to be any type of luminous companion.

If SZ Lyn B is a compact star, its mass exceeds the Chandrasekhar limit and falls within the typical range of NS masses, ruling out a WD interpretation. Moreover, spectroscopic analysis reveals no broad WD absorption features near the Balmer lines in either LAMOST (Figure 1) or high-resolution spectra ([Adassuriya et al. 2024](#)). A single WD companion is therefore strongly disfavoured. A black hole companion is likewise ruled out by the inferred mass, which lies well below the typical black hole mass range. A NS thus emerges as the most straightforward explanation, and we adopt this as our default assumption throughout the paper.

We therefore propose SZ Lyn B as a NS candidate—the most parsimonious interpretation consistent with all observational constraints. We note that the possibility of a close binary containing two low-mass WDs is not directly ruled out by current observations. However, given that SZ Lyn A has an age of 1.254 Gyr (Table 4) and that the WD progenitors would have had main-sequence lifetimes of at most a few Gyr, both WDs would be older than SZ Lyn A, and SZ Lyn B could not have been captured by SZ Lyn A. Therefore, SZ Lyn B is unlikely to be a close binary containing two low-mass WDs. Crucially, at periastron, the radius of SZ Lyn A remains well within its Roche lobe, indicating negligible mass transfer—which naturally explains the absence of detectable accretion-powered X-ray or gamma-ray emission from the NS candidate.

2.5. The Future Prospects of SZ Lyn

Future observations will be essential for confirming the nature of SZ Lyn B. Precise astrometry from Gaia DR4 and subsequent missions can refine the orbital inclination and companion mass, while radio observations with the Five-hundred-meter Aperture Spherical Telescope (FAST) may detect potential radio signatures despite the wide separation. These efforts will help validate the neutron star interpretation and further constrain the system’s evolutionary history. SZ Lyn represents one of the first δ Scuti binaries with a NS candidate identified through the synergy of asteroseismology and dynamics, highlighting the potential of this approach to uncover non-accreting compact objects.

3. CONCLUSIONS

We identify SZ Lyn as a noteworthy binary system. Asteroseismic modeling of the primary component, SZ Lyn A, successfully reproduces its six pulsation frequencies, yielding precise fundamental parameters: mass $M = 1.83_{-0.01}^{+0.06} M_{\odot}$,

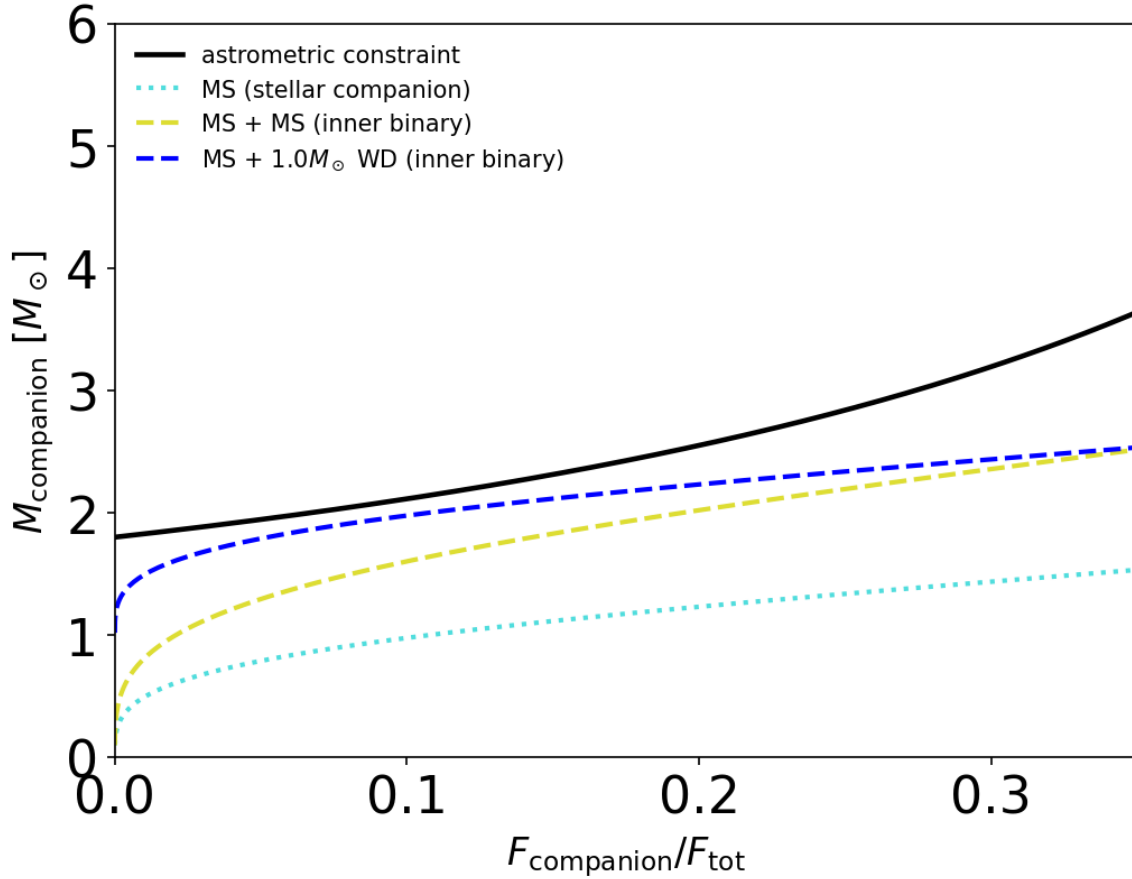


Figure 5. Constraints on the mass of the unseen companion in SZ Lyn as a function of the G -band flux ratio. The solid black line shows the constraint from the astrometric mass function, setting a primary mass $M_1 = 1.83 M_\odot$; a completely dark companion would imply $M_2 \approx 1.76 M_\odot$. If the companion contributes any light, its astrometrically inferred mass increases. The dotted cyan line shows the expected flux ratio and mass for a single main-sequence (MS) companion, which always lies below the black line, ruling out any single MS companion as the explanation for the observed orbit. The same holds for an equal-mass inner binary (yellow dashed). Even an inner binary composed of a $1.0 M_\odot$ white dwarf (WD) and an MS star (blue dashed) has a mass-to-light ratio too low to match the astrometric mass function. This leaves a single NS or a WD-WD binary as the only viable companions.

radius $R = 2.899 \pm 0.027 R_\odot$, luminosity $L = 16.111^{+0.721}_{-0.354} L_\odot$, central hydrogen abundance $X_c = 0.089^{+0.032}_{-0.005}$, and age $= 1.254^{+0.079}_{-0.024}$ Gyr. These results indicate that SZ Lyn A is a post-main-sequence HADS.

The companion, SZ Lyn B, orbits in a low-eccentricity orbit ($e = 0.18$). Using the orbital inclination derived from Gaia astrometry ($i = 38.67 \pm 0.29^\circ$), we obtain companion masses of $M_2 = 1.76^{+0.042}_{-0.042} M_\odot$ from radial velocity analysis and $M_2 = 2.07^{+0.045}_{-0.045} M_\odot$ from pulsation timing variations, with corresponding orbital separations of $a_{\text{RV}} = 3.342^{+0.046}_{-0.046}$ au and $a_{O-C} = 3.449^{+0.035}_{-0.035}$ au, respectively. These mass estimates place the companion well above the Chandrasekhar limit and within the typical mass range of NSs.

Multiple lines of evidence rule out luminous companions: the astrometric mass function excludes single main-sequence stars, equal-mass inner binaries, and WD–main-sequence binaries; the absence of antiphase spectral lines, a single-component $O - C$ diagram, and a spectral energy distribution fully consistent with an A-type star further support this conclusion. A WD companion is disfavored by both the mass exceeding the Chandrasekhar limit and the lack of broad Balmer absorption features, while a black hole is ruled out by the inferred mass being far below the typical black hole mass range. The possibility of a double WD binary remains observationally unconstrained but is deemed unlikely based on age arguments and capture considerations. Together, these constraints point to a NS as the most parsimonious interpretation.

This system holds significant astrophysical value. It represents a rare configuration—a wide, near-circular binary containing a pulsating star and a quiescent NS candidate—offering new constraints on supernova kick models and enabling potential studies of asteroseismology in strong gravity regimes. The discovery also demonstrates the effectiveness of combining asteroseismology with dynamical methods (radial velocity and light-travel time effect) for identifying non-accreting compact objects in wide binaries.

This work is supported by the International Cooperation Projects of the National Key R&D Program (No. 2022YFE0127300), the National Natural Science Foundation of China (No. 11933008), the Young Talent Project of “Yunnan Revitalization Talent Support Program” in Yunnan Province, the basic research project of Yunnan Province (Grant No. 202201AT070092), CAS “Light of West China” Program. This work has made use of data from the European Space Agency (ESA) mission Gaia. (<https://www.cosmos.esa.int/gaia>), processed by the Gaia Data Processing and Analysis Consortium (DPAC; <https://www.cosmos.esa.int/web/gaia/dpac/consortium>). Funding for the DPAC has been provided by national institutions, in particular the institutions participating in the *Gaia* Multilateral Agreement. The *TESS* data presented in this paper were obtained from the Mikulski Archive for Space Telescopes (MAST) at the Space Telescope Science Institute (STScI). STScI is operated by the Association of Universities for Research in Astronomy, Inc. Support to MAST for these data is provided by the NASA Office of Space Science. Funding for the *TESS* mission is provided by the NASA Explorer Program.

Facilities: TESS, LAMOST

Software: astropy (Astropy Collaboration et al. 2013, 2018), MESA (Paxton et al. 2011, 2013, 2015, 2018), *Pulse_Adipls* (Christensen-Dalsgaard 2008)

APPENDIX

A. LIGHT CURVE DATA AND FREQUENCY ANALYSIS

SZ Lyn was observed by the TESS mission in Sectors 20 and 47 with a 120-second cadence. We retrieved the Presearch Data Conditioning Simple Aperture Photometry (PDCSAP) flux from the Mikulski Archive for Space Telescopes (MAST) and converted it to magnitudes (Figure 6).

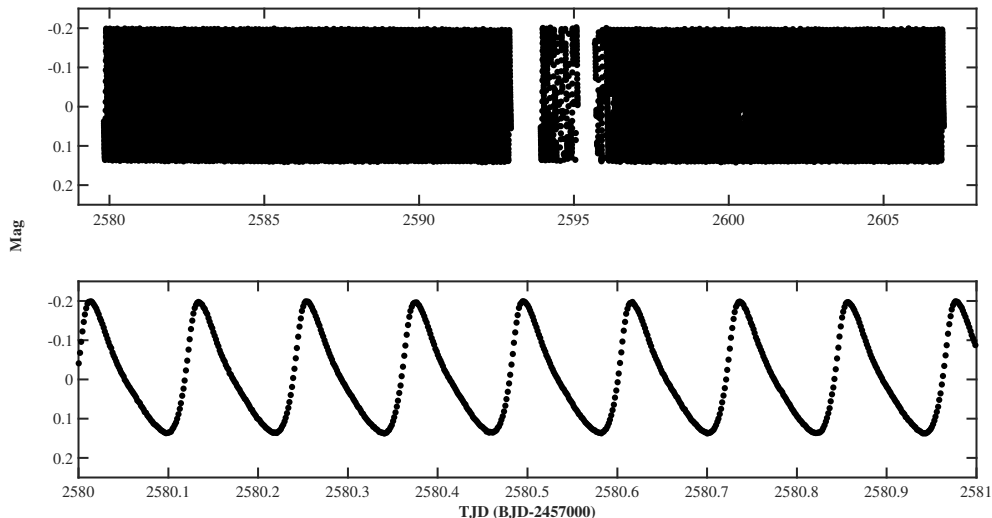


Figure 6. Light curve of SZ Lyn from TESS Sector 20. The lower panel shows a one-day zoom for clarity.

Table 2. Pulsating frequencies of SZ Lyn.

ID	Frequency (c/d)	Frequency (μHz)	error (c/d)	Amplitude (mag)	error (mag)	SNR
F_1	8.2961135	96.0198326	0.0000011	0.1453108	0.0000084	10720.80
F_2	14.53716	168.25419	0.00034	0.0004918	0.0000084	54.99
F_3	37.17183	430.22954	0.00035	0.0004795	0.0000084	42.06
F_4	32.6165	377.5065	0.0015	0.0001110	0.0000084	7.40
F_5	4.58526	53.07015	0.00060	0.0002833	0.0000084	21.62
F_6	55.3391	640.4991	0.0039	0.0000436	0.0000084	5.17

To analyze the pulsation properties of SZ Lyn, we subtracted the light-curve model from the TESS light curves. The frequency resolution for this dataset is $\delta f = 1/\Delta T \approx 0.0368$ c/d, where ΔT denotes the total observational time span covering sectors 45 and 46. We performed a detailed pulsation analysis of the light-curve residuals using multi-frequency analysis with the *Period 04* software (Lenz & Breger 2005). As no pulsation signals were detected above 120 c/d, subsequent frequency extraction was restricted to the range 0–120 c/d (Figure 7).

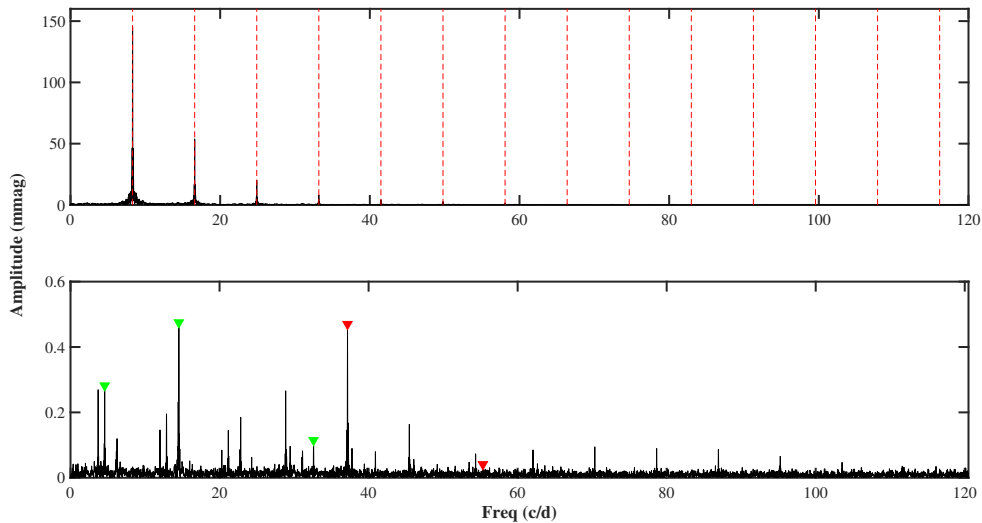


Figure 7. Frequency spectrum of SZ Lyn. Top panel: Red dotted vertical lines (0–120 c/d) mark the fundamental mode (highest amplitude) and its harmonics. Lower panel: The six independent pulsation frequencies, listed in Table 2, with green triangles indicating non-radial modes identified by Adassuriya et al. (2021) and red triangles denoting new frequencies detected in this work.

At each iteration, we identified the highest-amplitude frequency and performed a multi-period least-squares fit including all previously detected frequencies. The data were then pre-whitened using this solution, and the resulting residuals formed the basis for subsequent analysis. This process iterated until residuals satisfied the signal-to-noise criterion $S/N \geq 4.0$ (Breger et al. 1993). Following Montgomery & O’Donoghue (1999), we computed the noise within a 1 c/d bandwidth centered on each frequency, and determined corresponding amplitudes and their uncertainties.

We examined the extracted frequencies to identify linear combination frequencies of the form $F_k = mF_i + nF_j$ (Pápics 2012; Kurtz et al. 2015), where m and n are integers, F_i and F_j represent parent frequencies, F_k denotes the combination frequency. A peak is classified as a combination if it satisfies two criteria: (1) both parent frequencies have amplitudes greater than the presumed combination term, and (2) the difference between observed and predicted frequencies is smaller than the frequency resolution δf (Loumos & Deeming 1978; Lee et al. 2019). Finally, Six independent frequencies (F_1 – F_6) were identified (Table 2), including two tentative new frequencies (F_3 , F_6) (red

triangles in Figure 7). The remaining frequencies correspond to those reported by Adassuriya et al. (2021) within our frequency resolution.

B. STELLAR MODEL AND ASTEROSEISMIC ANALYSIS FOR SZ LYN

B.1. *Input Physics*

We thus utilize the stellar evolution code Modules for Experiments in Stellar Astrophysics (MESA, version r22.11.1), developed by Paxton et al. (2011, 2013, 2015, 2018), to compute evolutionary and pulsational models for component B. Specifically, for generating stellar evolution models and calculating the adiabatic frequencies of radial and non-radial modes, we employ the *pulse_adipls* (Christensen-Dalsgaard 2008) submodule in MESA. Our calculations adopt the 2005 update of the OPAL equation of state tables (Rogers & Nayfonov 2002). For opacity, we utilize the OPAL high-temperature tables from Iglesias & Rogers (1996) and the low-temperature tables from Ferguson et al. (2005). We assume the initial metallicity is identical to the solar value (Asplund et al. 2009). Convective zones are treated using the classical mixing-length theory (Böhm-Vitense 1958) with a mixing-length parameter $\alpha = 1.90$ (Paxton et al. 2011).

To model convective core overshooting, we adopt an exponentially decaying prescription for the overshooting - mixing diffusion coefficient (Freytag et al. 1996; Herwig 2000):

$$D_{\text{ov}} = D_0 \exp\left(\frac{-2z}{f_{\text{ov}} H_p}\right), \quad (\text{B1})$$

where D_0 is the diffusion coefficient at the edge of the convective core, z is the distance into the radiative zone from the edge, f_{ov} is an adjustable parameter describing the efficiency of overshooting, and H_p is the pressure scale height. The lower limit of the diffusion coefficient is set to $D_{\text{ov}}^{\text{limit}} = 1 \times 10^{-2} \text{ cm}^2 \text{ s}^{-1}$ (Chen et al. 2019), below which overshooting is neglected in our models. In addition, we do not include elemental diffusion, stellar rotation, and magnetic fields in the stellar structure and evolution calculations.

B.2. *Grid of Stellar Models for SZ Lyn A*

Stellar evolution paths and internal structures depend critically on the initial mass M , initial chemical composition (X, Y, Z) , and the convective overshooting parameter f_{ov} . Following Li et al. (2018), we adopt the helium abundance relation $Y = 0.249 + 1.33Z$, thereby reducing the number of independent parameters to M , Z , and f_{ov} . We perform a grid search over stellar masses M from 1.70 to 2.00 M_{\odot} with a step of 0.01 M_{\odot} according our results of Adassuriya et al. (2021), and metallicities Z from 0.010 to 0.020 in steps of 0.001. For the overshooting at the top of the convective core, we follow the method of Chen et al. (2019) to take the case of moderate overshooting ($f_{\text{ov}} = 0.01$).

Each star in the grid is computed from the zero-age-main-sequence to the post-main-sequence stage ($X_c = 1 \times 10^{-5}$). The effective temperatures of δ Scuti normally vary between 6000 K and 9800 K (Aerts et al. 2010). we restrict the effective temperature of stellar models inside this range. Luminosity and radius are constrained to $1.24 < \log(L/L_{\odot}) < 1.53$ and $0.39 < \log(R/R_{\odot}) < 0.53$, based on results from our light curve modeling. As a star moves along its evolutionary track into this region, the adiabatic frequencies of the radial ($\ell = 0$) and non-radial ($\ell = 1, 2$, and 3) oscillations are calculated for the structure model at each stage of its evolution.

Additionally, we also include stellar rotation as a fourth adjustable parameter, varying the rotation velocity V_{rot} from 1 to 20 km s^{-1} in steps of 1 km s^{-1} due to the component B's rotation velocity is $v_{\text{rot}} = 10 \text{ km s}^{-1}$ (Adassuriya et al. 2024). For each pulsation mode at a given P_{rot} , rotational splitting produces $2l + 1$ frequency components according to:

$$\nu_{l,n,m} = \nu_{l,n} + m\delta\nu_{l,n} = \nu_{l,n} + \beta_{l,n} \frac{m}{P_{\text{rot}}} \quad (\text{B2})$$

(Saio 1981; Dziembowski & Goode 1992; Aerts et al. 2010), where $\delta\nu_{l,n}$ is the rotational splitting frequency and $\beta_{l,n}$ determines the splitting magnitude. For uniformly rotating stars, $\beta_{l,n}$ is given by Aerts et al. (2010):

$$\beta_{l,n} = \frac{\int_0^R (\xi_r^2 + L^2 \xi_h^2 - 2\xi_r \xi_h - \xi_h^2) r^2 \rho dr}{\int_0^R (\xi_r^2 + L^2 \xi_h^2) r^2 \rho dr}, \quad (\text{B3})$$

where ξ_r and ξ_h are the radial and horizontal displacement eigenfunctions, ρ is the local density, and $L^2 = l(l+1)$. According to Equation B2, each dipole mode splits into three different components, corresponding to modes with m

Table 3. Comparisons between model frequencies of best-fitting model (Model A55) and observations.

ID	F_{mod} (μHz)	F_{obs} (μHz)	(ℓ, n_p, n_g, m)	$ F_{\text{mod}} - F_{\text{obs}} $ (μHz)
F_1	96.2190	96.0185	(0, 0, 0, 0)	0.2005
F_2	168.3562	168.2291	(2, -2, 2, -1)	0.1271
F_3	430.4194	430.2295	(1, 11, 0, -1)	0.1899
F_4	377.4836	377.5462	(2, 8, 0, 1)	0.0626
F_5	53.0423	53.0555	(3, 0, -14, -3)	0.0132
F_6	640.5245	640.4991	(3, 16, 0, 0)	0.0254

NOTE— F_{obs} is the observed frequency. F_{mod} is the model frequency. (ℓ, n_p, n_g, m) are the spherical harmonic degree, the radial orders in the p-mode propagation zone, the radial orders in the g-mode propagation zone, and the azimuthal number of the model frequency.

Table 4. Fundamental parameters of the component A of SZ Lyn.

Parameters	Single-star Models
Z	0.015–0.018 (0.015 $^{+0.003}_{-0.000}$)
M (M_{\odot})	1.82–1.89 (1.83 $^{+0.06}_{-0.01}$)
V_{rot} (kms^{-1})	2–20 (9 $^{+11}_{-7}$)
T_{eff} (K)	6732–6842 (6791 $^{+51}_{-58}$)
$\log(g)$ (cms^{-2})	3.774–3.782 (3.776 $^{+0.006}_{-0.002}$)
R (R_{\odot})	2.899–2.906 (2.899 $^{+0.027}_{-0.000}$)
L (L_{\odot})	15.758–16.833 (16.112 $^{+0.721}_{-0.354}$)
τ_0 (hr)	3.748–3.759 (3.750 $^{+0.009}_{-0.002}$)
X_c	0.084–0.121 (0.089 $^{+0.032}_{-0.005}$)
Age (Gyr)	1.230–1.333 (1.254 $^{+0.079}_{-0.024}$)

NOTE— V_{rot} denotes the rotation velocity. τ_0 is the acoustic radius. X_c is the central hydrogen abundance.

= -1, 0, and +1, respectively. Each quadrupole mode splits into five different components, corresponding to modes with $m = -2, -1, 0, +1, \text{ and } +2$, respectively.

B.3. Fitting Results of SZ Lyn B

We compare model frequencies with spherical degrees $l = 0, 1, 2, \text{ and } 3$ to the observed frequencies $F_1, F_2, F_3, F_4, F_5, \text{ and } F_6$ to identify the optimal model. The goodness of fit is evaluated using:

$$S^2 = \frac{1}{k} \sum_{i=1}^k |f_{\text{model},i} - f_{\text{obs},i}|^2, \quad (\text{B4})$$

where $f_{\text{obs},i}$ is the i -th observed frequency, $f_{\text{model},i}$ is the corresponding model frequency, and k is the number of observed modes. The frequencies F_3 and F_6 could not be precisely identified in advance; therefore, the nearest theoretical frequencies were assigned to represent them in the model.

Figures 8 and 9 display the variation of the goodness-of-fit S_m^2 across different physical parameters. Each dot in the figures represents one minimum value of S^2 along one evolutionary track, denoted as S_m^2 . Horizontal lines in both figures indicate $S_m^2 = 0.10$, corresponding to the squared value of the frequency resolution δf . Dots above this threshold correspond to 84 candidate models that are listed in Table 5. Model A55 achieves the global minimum $S_m^2 = 0.0162$, establishing it as the optimal solution. This best-fitting model is highlighted by red dots in Figures 8 and 9.

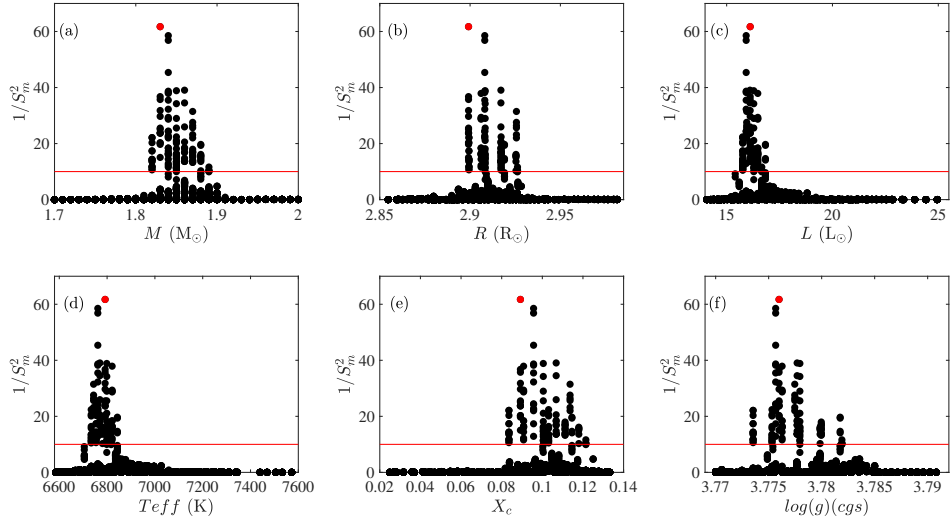


Figure 8. This visualization presents the fitting metric S_m^2 and physical parameters: stellar mass (M), radius (R), luminosity (L), effective temperature (T_{eff}), central hydrogen abundance (X_c), and gravitational acceleration ($\log g$) with a red horizontal line marking the threshold $S_m^2 = 0.10$, where black dots indicate the minimum S_m^2 for each model while the red dot identifies the minimum S_m^2 of the best-fitting model.

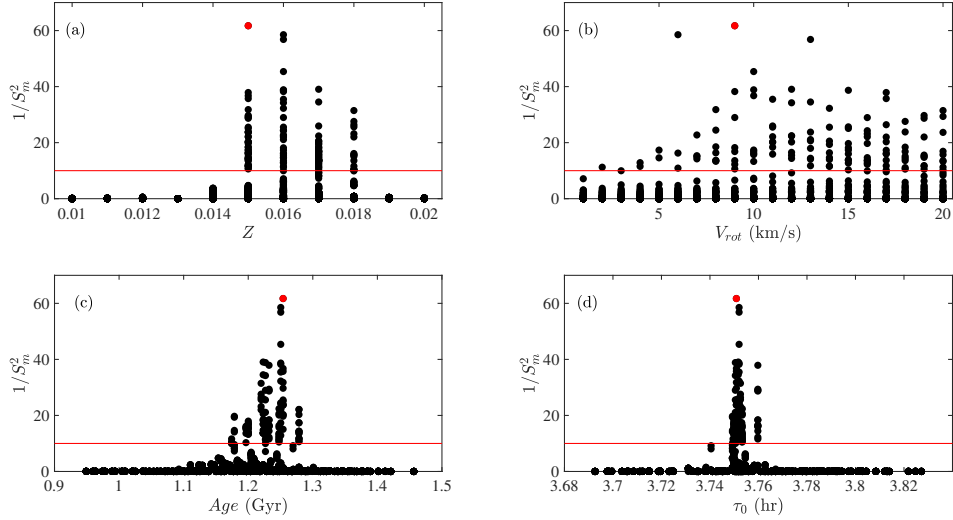


Figure 9. This visualization presents the fitting results S_m^2 alongside key physical parameters: metallicity (Z), stellar rotation velocity (V_{rot}), stellar age (Age), and acoustic radius (τ_0). A red horizontal line marks the threshold $S_m^2 = 0.10$. Black dots denote the minimum S_m^2 for each model, while a red dot identifies the minimum S_m^2 for the best-fitting model.

Figures 8 (a)–(c) display the variation of S_m^2 versus stellar mass (M), radius (R), and luminosity (L). These parameters demonstrate excellent convergence with best-fit values $M = 1.83^{+0.06}_{-0.01} M_{\odot}$, $R = 2.899^{+0.027}_{-0.000} R_{\odot}$, and $L = 16.111^{+0.721}_{-0.354} L_{\odot}$. Meanwhile, Figures 8 (d)–(f) show S_m^2 as functions of effective temperature (T_{eff}), gravitational acceleration ($\log g$), and central hydrogen abundance (X_c). The parameters effective temperature and gravitational acceleration exhibit tight constraints: $T_{\text{eff}} = 6791^{+51}_{-58}$ Gyr and $\log g = 3.776^{+0.006}_{-0.002} \text{ cm s}^{-2}$. In contrast, the central hydrogen abundance spans a broader range $X_c = 0.089^{+0.032}_{-0.005}$.

Figures 9 (a)–(d) depict the variation of S_m^2 with metallicity (Z), rotation velocity (V_{rot}), stellar age (Age) and acoustic radius (τ_0). Excellent convergence is observed for metallicity (Z), stellar age (Age) and acoustic radius (τ_0)

with best-fit values $Z = 0.016_{-0.001}^{+0.008}$, $\text{Age} = 1.254_{-0.024}^{+0.079}$ Gyr and $\tau_0 = 3.750_{-0.002}^{+0.009}$ hr, while the stellar rotation shows a broader distribution $T_{\text{eff}} = 9_{-7}^{+11}$ km/s.

Table 3 presents a comparison between the observed frequencies and those of the best-fitting model (Model A55). Based on this comparison, new frequencies F_5 and F_6 are identified as two non radial modes with $l=1$ and 3, respectively. F_1 is classified as a radial mode, while F_2 , F_3 , and F_4 are recognized as non radial modes with $l=2$ and 3 that is matched with the results of mode identification in Adassuriya et al. (2021). The asteroseismically derived parameters of component A in SZ Lyn are therefore listed in Column 2 of Table 4.

Table 5. Candidate models with $S_m^2 < 0.10$.

Mode ID	X_c	M (M_\odot)	T_{eff} (K)	$\log g$ (cms^{-2})	R (R_\odot)	L (L_\odot)	Age (Gyr)	Z	V_{rot} (km/s)	τ_0 (hr)	S_m^2
A1	0.0957	1.84	6761	3.776	2.908	15.922	1.250	0.0160	7	3.752	0.0440
A2	0.0957	1.84	6761	3.776	2.908	15.922	1.250	0.0160	15	3.752	0.0258
A3	0.0957	1.84	6761	3.776	2.908	15.922	1.250	0.0160	14	3.752	0.0310
A4	0.0957	1.84	6761	3.776	2.908	15.922	1.250	0.0160	16	3.752	0.0412
A5	0.0957	1.84	6761	3.776	2.908	15.922	1.250	0.0160	10	3.752	0.0220
A6	0.0957	1.84	6761	3.776	2.908	15.922	1.250	0.0160	6	3.752	0.0171
A7	0.0957	1.84	6761	3.776	2.908	15.922	1.250	0.0160	9	3.752	0.0261
A8	0.0957	1.84	6761	3.776	2.908	15.922	1.250	0.0160	8	3.752	0.0409
A9	0.0957	1.84	6761	3.776	2.908	15.922	1.250	0.0160	11	3.752	0.0282
A10	0.0957	1.84	6761	3.776	2.908	15.922	1.250	0.0160	4	3.752	0.0777
A11	0.0957	1.84	6761	3.776	2.908	15.922	1.250	0.0160	17	3.752	0.0455
A12	0.0957	1.84	6761	3.776	2.908	15.922	1.250	0.0160	12	3.752	0.0446
A13	0.0957	1.84	6761	3.776	2.908	15.922	1.250	0.0160	13	3.752	0.0176
A14	0.0957	1.84	6761	3.776	2.908	15.922	1.250	0.0160	5	3.752	0.0577
A15	0.0836	1.82	6754	3.774	2.899	15.757	1.279	0.0150	13	3.753	0.0850
A16	0.0836	1.82	6754	3.774	2.899	15.757	1.279	0.0150	8	3.753	0.0730
A17	0.0836	1.82	6754	3.774	2.899	15.757	1.279	0.0150	16	3.753	0.0452
A18	0.0836	1.82	6754	3.774	2.899	15.757	1.279	0.0150	18	3.753	0.0696
A19	0.0836	1.82	6754	3.774	2.899	15.757	1.279	0.0150	19	3.753	0.0846
A20	0.0836	1.82	6754	3.774	2.899	15.757	1.279	0.0150	11	3.753	0.0452
A21	0.0836	1.82	6754	3.774	2.899	15.757	1.279	0.0150	6	3.753	0.0917
A22	0.0836	1.82	6754	3.774	2.899	15.757	1.279	0.0150	7	3.753	0.0704
A23	0.0836	1.82	6754	3.774	2.899	15.757	1.279	0.0150	12	3.753	0.0696
A24	0.0836	1.82	6754	3.774	2.899	15.757	1.279	0.0150	15	3.753	0.0576
A25	0.0836	1.82	6754	3.774	2.899	15.757	1.279	0.0150	14	3.753	0.0863
A26	0.0836	1.82	6754	3.774	2.899	15.757	1.279	0.0150	10	3.753	0.0576
A27	0.0836	1.82	6754	3.774	2.899	15.757	1.279	0.0150	9	3.753	0.0942
A28	0.0836	1.82	6754	3.774	2.899	15.757	1.279	0.0150	17	3.753	0.0492
A29	0.0836	1.82	6754	3.774	2.899	15.757	1.279	0.0150	20	3.753	0.0736
A30	0.1005	1.85	6799	3.778	2.908	16.281	1.227	0.0160	12	3.750	0.0292
A31	0.1005	1.85	6799	3.778	2.908	16.281	1.227	0.0160	11	3.750	0.0392
A32	0.1005	1.85	6799	3.778	2.908	16.281	1.227	0.0160	5	3.750	0.0686
A33	0.1005	1.85	6799	3.778	2.908	16.281	1.227	0.0160	4	3.750	0.0867
A34	0.1005	1.85	6799	3.778	2.908	16.281	1.227	0.0160	6	3.750	0.0614
A35	0.1005	1.85	6799	3.778	2.908	16.281	1.227	0.0160	7	3.750	0.0652
A36	0.1005	1.85	6799	3.778	2.908	16.281	1.227	0.0160	2	3.750	0.0890
A37	0.1005	1.85	6799	3.778	2.908	16.281	1.227	0.0160	8	3.750	0.0738
A38	0.1005	1.85	6799	3.778	2.908	16.281	1.227	0.0160	9	3.750	0.0345
A39	0.1005	1.85	6799	3.778	2.908	16.281	1.227	0.0160	10	3.750	0.0257
A40	0.1005	1.85	6799	3.778	2.908	16.281	1.227	0.0160	13	3.750	0.0474
A41	0.1005	1.85	6799	3.778	2.908	16.281	1.227	0.0160	16	3.750	0.0781
A42	0.1005	1.85	6799	3.778	2.908	16.281	1.227	0.0160	14	3.750	0.0681
A43	0.1005	1.85	6799	3.778	2.908	16.281	1.227	0.0160	15	3.750	0.0551
A44	0.1005	1.85	6799	3.778	2.908	16.281	1.227	0.0160	17	3.750	0.0626

Continued

Table 5 – continued

Mode ID	X_c	$M (M_\odot)$	$T_{\text{eff}} (K)$	$\log g (\text{cgs}^{-2})$	$R (R_\odot)$	$L (L_\odot)$	Age (Gyr)	Z	$V_{\text{rot}} (\text{km/s})$	$\tau_0 (\text{hr})$	S_m^2
A45	0.0892	1.83	6792	3.776	2.899	16.112	1.254	0.0150	11	3.751	0.0493
A46	0.0892	1.83	6792	3.776	2.899	16.112	1.254	0.0150	13	3.751	0.0421
A47	0.0892	1.83	6792	3.776	2.899	16.112	1.254	0.0150	10	3.751	0.0272
A48	0.0892	1.83	6792	3.776	2.899	16.112	1.254	0.0150	15	3.751	0.0399
A49	0.0892	1.83	6792	3.776	2.899	16.112	1.254	0.0150	19	3.751	0.0337
A50	0.0892	1.83	6792	3.776	2.899	16.112	1.254	0.0150	18	3.751	0.0420
A51	0.0892	1.83	6792	3.776	2.899	16.112	1.254	0.0150	16	3.751	0.0507
A52	0.0892	1.83	6792	3.776	2.899	16.112	1.254	0.0150	17	3.751	0.0280
A53	0.0892	1.83	6792	3.776	2.899	16.112	1.254	0.0150	8	3.751	0.0315
A54	0.0892	1.83	6792	3.776	2.899	16.112	1.254	0.0150	20	3.751	0.0423
A55	0.0892	1.83	6792	3.776	2.899	16.112	1.254	0.0150	9	3.751	0.0162
A56	0.0892	1.83	6792	3.776	2.899	16.112	1.254	0.0150	12	3.751	0.0494
A57	0.0892	1.83	6792	3.776	2.899	16.112	1.254	0.0150	7	3.751	0.0664
A58	0.0892	1.83	6792	3.776	2.899	16.112	1.254	0.0150	14	3.751	0.0392
A59	0.0908	1.84	6821	3.776	2.906	16.471	1.232	0.0150	15	3.760	0.0625
A60	0.0908	1.84	6821	3.776	2.906	16.471	1.232	0.0150	18	3.760	0.0543
A61	0.0908	1.84	6821	3.776	2.906	16.471	1.232	0.0150	13	3.760	0.0693
A62	0.0908	1.84	6821	3.776	2.906	16.471	1.232	0.0150	19	3.760	0.0348
A63	0.0908	1.84	6821	3.776	2.906	16.471	1.232	0.0150	20	3.760	0.0341
A64	0.0908	1.84	6821	3.776	2.906	16.471	1.232	0.0150	12	3.760	0.0605
A65	0.0908	1.84	6821	3.776	2.906	16.471	1.232	0.0150	11	3.760	0.0544
A66	0.0908	1.84	6821	3.776	2.906	16.471	1.232	0.0150	14	3.760	0.0863
A67	0.0908	1.84	6821	3.776	2.906	16.471	1.232	0.0150	9	3.760	0.0818
A68	0.0908	1.84	6821	3.776	2.906	16.471	1.232	0.0150	10	3.760	0.0618
A69	0.0908	1.84	6821	3.776	2.906	16.471	1.232	0.0150	16	3.760	0.0345
A70	0.0908	1.84	6821	3.776	2.906	16.471	1.232	0.0150	17	3.760	0.0264
A71	0.0908	1.84	6821	3.776	2.906	16.471	1.232	0.0150	8	3.760	0.0611
A72	0.1068	1.86	6770	3.778	2.917	16.103	1.223	0.0170	19	3.752	0.0678
A73	0.1068	1.86	6770	3.778	2.917	16.103	1.223	0.0170	17	3.752	0.0728
A74	0.1068	1.86	6770	3.778	2.917	16.103	1.223	0.0170	8	3.752	0.0540
A75	0.1068	1.86	6770	3.778	2.917	16.103	1.223	0.0170	20	3.752	0.0591
A76	0.1068	1.86	6770	3.778	2.917	16.103	1.223	0.0170	16	3.752	0.0732
A77	0.1068	1.86	6770	3.778	2.917	16.103	1.223	0.0170	15	3.752	0.0729
A78	0.1068	1.86	6770	3.778	2.917	16.103	1.223	0.0170	10	3.752	0.0594
A79	0.1068	1.86	6770	3.778	2.917	16.103	1.223	0.0170	18	3.752	0.0735
A80	0.1068	1.86	6770	3.778	2.917	16.103	1.223	0.0170	14	3.752	0.0486
A81	0.1068	1.86	6770	3.778	2.917	16.103	1.223	0.0170	13	3.752	0.0290
A82	0.1068	1.86	6770	3.778	2.917	16.103	1.223	0.0170	11	3.752	0.0385
A83	0.1068	1.86	6770	3.778	2.917	16.103	1.223	0.0170	12	3.752	0.0256
A84	0.1068	1.86	6770	3.778	2.917	16.103	1.223	0.0170	9	3.752	0.0548
A85	0.1031	1.85	6734	3.775	2.917	15.761	1.248	0.0170	8	3.753	0.0749
A86	0.1031	1.85	6734	3.775	2.917	15.761	1.248	0.0170	12	3.753	0.0446
A87	0.1031	1.85	6734	3.775	2.917	15.761	1.248	0.0170	20	3.753	0.0888
A88	0.1031	1.85	6734	3.775	2.917	15.761	1.248	0.0170	19	3.753	0.0952
A89	0.1031	1.85	6734	3.775	2.917	15.761	1.248	0.0170	11	3.753	0.0497
A90	0.1031	1.85	6734	3.775	2.917	15.761	1.248	0.0170	13	3.753	0.0484
A91	0.1031	1.85	6734	3.775	2.917	15.761	1.248	0.0170	14	3.753	0.0610
A92	0.1031	1.85	6734	3.775	2.917	15.761	1.248	0.0170	15	3.753	0.0788
A93	0.1031	1.85	6734	3.775	2.917	15.761	1.248	0.0170	10	3.753	0.0635
A94	0.1031	1.85	6734	3.775	2.917	15.761	1.248	0.0170	16	3.753	0.0816
A95	0.1031	1.85	6734	3.775	2.917	15.761	1.248	0.0170	18	3.753	0.0903
A96	0.1031	1.85	6734	3.775	2.917	15.761	1.248	0.0170	9	3.753	0.0736
A97	0.1031	1.85	6734	3.775	2.917	15.761	1.248	0.0170	17	3.753	0.0851

Continued

Table 5 – continued

Mode ID	X_c	M (M_\odot)	T_{eff} (K)	$\log g$ (cms^{-2})	R (R_\odot)	L (L_\odot)	Age (Gyr)	Z	V_{rot} (km/s)	τ_0 (hr)	S_m^2
A98	0.1137	1.87	6743	3.777	2.926	15.947	1.220	0.0180	17	3.753	0.0379
A99	0.1137	1.87	6743	3.777	2.926	15.947	1.220	0.0180	16	3.753	0.0432
A100	0.1137	1.87	6743	3.777	2.926	15.947	1.220	0.0180	18	3.753	0.0363
A101	0.1137	1.87	6743	3.777	2.926	15.947	1.220	0.0180	15	3.753	0.0390
A102	0.1137	1.87	6743	3.777	2.926	15.947	1.220	0.0180	20	3.753	0.0318
A103	0.1137	1.87	6743	3.777	2.926	15.947	1.220	0.0180	19	3.753	0.0454
A104	0.1180	1.88	6781	3.780	2.925	16.301	1.197	0.0180	15	3.751	0.0972
A105	0.1180	1.88	6781	3.780	2.925	16.301	1.197	0.0180	20	3.751	0.0636
A106	0.1180	1.88	6781	3.780	2.925	16.301	1.197	0.0180	19	3.751	0.0643
A107	0.1180	1.88	6781	3.780	2.925	16.301	1.197	0.0180	16	3.751	0.0735
A108	0.1180	1.88	6781	3.780	2.925	16.301	1.197	0.0180	18	3.751	0.0662
A109	0.1180	1.88	6781	3.780	2.925	16.301	1.197	0.0180	17	3.751	0.0620
A110	0.1112	1.87	6807	3.780	2.917	16.465	1.200	0.0170	11	3.750	0.0629
A111	0.1112	1.87	6807	3.780	2.917	16.465	1.200	0.0170	9	3.750	0.0594
A112	0.1112	1.87	6807	3.780	2.917	16.465	1.200	0.0170	17	3.750	0.0579
A113	0.1112	1.87	6807	3.780	2.917	16.465	1.200	0.0170	12	3.750	0.0647
A114	0.1112	1.87	6807	3.780	2.917	16.465	1.200	0.0170	14	3.750	0.0716
A115	0.1112	1.87	6807	3.780	2.917	16.465	1.200	0.0170	13	3.750	0.0556
A116	0.1112	1.87	6807	3.780	2.917	16.465	1.200	0.0170	15	3.750	0.0720
A117	0.1112	1.87	6807	3.780	2.917	16.465	1.200	0.0170	10	3.750	0.0752
A118	0.1112	1.87	6807	3.780	2.917	16.465	1.200	0.0170	20	3.750	0.0752
A119	0.1112	1.87	6807	3.780	2.917	16.465	1.200	0.0170	18	3.750	0.0594
A120	0.1112	1.87	6807	3.780	2.917	16.465	1.200	0.0170	19	3.750	0.0661
A121	0.1214	1.89	6817	3.782	2.926	16.660	1.174	0.0180	17	3.750	0.0981
A122	0.1214	1.89	6817	3.782	2.926	16.660	1.174	0.0180	18	3.750	0.0946
A123	0.1214	1.89	6817	3.782	2.926	16.660	1.174	0.0180	20	3.750	0.0980
A124	0.1214	1.89	6817	3.782	2.926	16.660	1.174	0.0180	19	3.750	0.0860
A125	0.1146	1.88	6843	3.782	2.919	16.833	1.179	0.0170	14	3.749	0.0517
A126	0.1146	1.88	6843	3.782	2.919	16.833	1.179	0.0170	15	3.749	0.0508
A127	0.1146	1.88	6843	3.782	2.919	16.833	1.179	0.0170	13	3.749	0.0709
A128	0.1146	1.88	6843	3.782	2.919	16.833	1.179	0.0170	16	3.749	0.0683

V_{rot} is the rotation velocity. τ_0 is the acoustic radius. X_c is the central hydrogen abundance.

REFERENCES

- Abbott, B. P., Abbott, R., Abbott, T. D., et al. 2017, prl, 119, 161101, doi: [10.1103/PhysRevLett.119.161101](https://doi.org/10.1103/PhysRevLett.119.161101)
- Abdo, A. A., Ackermann, M., Ajello, M., et al. 2010, apjs, 187, 460, doi: [10.1088/0067-0049/187/2/460](https://doi.org/10.1088/0067-0049/187/2/460)
- Adassuriya, J. 2022, PhD thesis, University of Colombo, Sri Lanka
- Adassuriya, J., Ganesh, S., De Cat, P., Joshi, S., & Jayaratne, C. 2024, Bulletin de la Societe Royale des Sciences de Liege, 93, 470, doi: [10.25518/0037-9565.11753](https://doi.org/10.25518/0037-9565.11753)
- Adassuriya, J., Ganesh, S., Gutiérrez, J. L., et al. 2021, mnras, 502, 541, doi: [10.1093/mnras/staa3923](https://doi.org/10.1093/mnras/staa3923)
- Aerts, C., Christensen-Dalsgaard, J., & Kurtz, D. W. 2010, Asteroseismology, doi: [10.1007/978-1-4020-5803-5](https://doi.org/10.1007/978-1-4020-5803-5)
- Agerer, F., & Hubscher, J. 2003, Information Bulletin on Variable Stars, 5485, 1
- Asplund, M., Grevesse, N., Sauval, A. J., & Scott, P. 2009, ARA&A, 47, 481, doi: [10.1146/annurev.astro.46.060407.145222](https://doi.org/10.1146/annurev.astro.46.060407.145222)
- Astropy Collaboration, Robitaille, T. P., Tollerud, E. J., et al. 2013, A&A, 558, A33, doi: [10.1051/0004-6361/201322068](https://doi.org/10.1051/0004-6361/201322068)
- Astropy Collaboration, Price-Whelan, A. M., Sipőcz, B. M., et al. 2018, AJ, 156, 123, doi: [10.3847/1538-3881/aabc4f](https://doi.org/10.3847/1538-3881/aabc4f)
- Bardin, C., & Imbert, M. 1981, aap, 98, 198
- . 1984, aaps, 57, 249
- Barnes, T. G., I., & Moffett, T. J. 1975, aj, 80, 48, doi: [10.1086/111712](https://doi.org/10.1086/111712)
- Binnendijk, L. 1968, aj, 73, 29, doi: [10.1086/110591](https://doi.org/10.1086/110591)
- Böhm-Vitense, E. 1958, ZA, 46, 108
- Breger, M., Stich, J., Garrido, R., et al. 1993, aap, 271, 482

- Caraveo, P. A., Bignami, G. F., & Trümper, J. E. 1996, *aapr*, 7, 209, doi: [10.1007/s001590050004](https://doi.org/10.1007/s001590050004)
- Chen, X., Li, Y., & Zhang, X. 2019, *apj*, 887, 253, doi: [10.3847/1538-4357/ab585b](https://doi.org/10.3847/1538-4357/ab585b)
- Christensen-Dalsgaard, J. 2008, *Ap&SS*, 316, 113, doi: [10.1007/s10509-007-9689-z](https://doi.org/10.1007/s10509-007-9689-z)
- Derekas, A., Kiss, L. L., Székely, P., et al. 2003, *aap*, 402, 733, doi: [10.1051/0004-6361:20030291](https://doi.org/10.1051/0004-6361:20030291)
- Dziembowski, W. A., & Goode, P. R. 1992, *ApJ*, 394, 670, doi: [10.1086/171621](https://doi.org/10.1086/171621)
- Ferguson, J. W., Alexander, D. R., Allard, F., et al. 2005, *ApJ*, 623, 585, doi: [10.1086/428642](https://doi.org/10.1086/428642)
- Fernley, J. A., Jameson, R. F., & Sherrington, M. R. 1984, *MNRAS*, 208, 853, doi: [10.1093/mnras/208.4.853](https://doi.org/10.1093/mnras/208.4.853)
- Freytag, B., Ludwig, H. G., & Steffen, M. 1996, *A&A*, 313, 497
- Gazeas, K. D., Niarchos, P. G., & Boutsia, K. A. 2004, *Communications in Asteroseismology*, 144, 26
- Haberl, F. 2007, *apss*, 308, 181, doi: [10.1007/s10509-007-9342-x](https://doi.org/10.1007/s10509-007-9342-x)
- Herwig, F. 2000, *A&A*, 360, 952, doi: [10.48550/arXiv.astro-ph/0007139](https://doi.org/10.48550/arXiv.astro-ph/0007139)
- Hubscher, J., Braune, W., & Lehmann, P. B. 2013, *Information Bulletin on Variable Stars*, 6048, 1
- Hubscher, J., & Lehmann, P. B. 2012, *Information Bulletin on Variable Stars*, 6026, 1
- Hubscher, J., Lehmann, P. B., Monninger, G., Steinbach, H.-M., & Walter, F. 2010, *Information Bulletin on Variable Stars*, 5918, 1
- Hubscher, J., Paschke, A., & Walter, F. 2005, *Information Bulletin on Variable Stars*, 5657, 1
- . 2006, *Information Bulletin on Variable Stars*, 5731, 1
- Hubscher, J., Steinbach, H.-M., & Walter, F. 2009a, *Information Bulletin on Variable Stars*, 5889, 1
- . 2009b, *Information Bulletin on Variable Stars*, 5874, 1
- Hubscher, J., & Walter, F. 2007, *Information Bulletin on Variable Stars*, 5761, 1
- Iglesias, C. A., & Rogers, F. J. 1996, *ApJ*, 464, 943, doi: [10.1086/177381](https://doi.org/10.1086/177381)
- Iglesias-Marzoa, R., López-Morales, M., & Jesús Arévalo Morales, M. 2015, *pasp*, 127, 567, doi: [10.1086/682056](https://doi.org/10.1086/682056)
- Irwin, J. B. 1952, *apj*, 116, 211, doi: [10.1086/145604](https://doi.org/10.1086/145604)
- Klingenberg, G., Dvorak, S. W., & Robertson, C. W. 2006, *Information Bulletin on Variable Stars*, 5701, 1
- Koleva, M., Prugniel, P., Bouchard, A., & Wu, Y. 2009, *aap*, 501, 1269, doi: [10.1051/0004-6361/200811467](https://doi.org/10.1051/0004-6361/200811467)
- Kurtz, D. W., Shibahashi, H., Murphy, S. J., Bedding, T. R., & Bowman, D. M. 2015, *MNRAS*, 450, 3015, doi: [10.1093/mnras/stv868](https://doi.org/10.1093/mnras/stv868)
- Lee, J. W., Hong, K., & Kristiansen, M. H. 2019, *AJ*, 157, 17, doi: [10.3847/1538-3881/aaf0fb](https://doi.org/10.3847/1538-3881/aaf0fb)
- Lenz, P., & Breger, M. 2005, *Communications in Asteroseismology*, 146, 53, doi: [10.1553/cia146s53](https://doi.org/10.1553/cia146s53)
- Li, L.-J., & Qian, S.-B. 2013, *pasj*, 65, 116, doi: [10.1093/pasj/65.6.116](https://doi.org/10.1093/pasj/65.6.116)
- Li, T., Bedding, T. R., Huber, D., et al. 2018, *MNRAS*, 475, 981, doi: [10.1093/mnras/stx3079](https://doi.org/10.1093/mnras/stx3079)
- Lorimer, D. R. 2008, *Living Reviews in Relativity*, 11, 8, doi: [10.12942/lrr-2008-8](https://doi.org/10.12942/lrr-2008-8)
- Loumos, G. L., & Deeming, T. J. 1978, *Ap&SS*, 56, 285, doi: [10.1007/BF01879560](https://doi.org/10.1007/BF01879560)
- Moffett, T. J., Barnes, Thomas G., I., Fekel, Francis C., J., Jefferys, W. H., & Achtermann, J. M. 1988, *aj*, 95, 1534, doi: [10.1086/114749](https://doi.org/10.1086/114749)
- Montgomery, M. H., & O'Donoghue, D. 1999, *Delta Scuti Star Newsletter*, 13, 28
- Niu, J.-S., Zhang, Y., & Xue, H.-F. 2026, *arXiv e-prints*, arXiv:2601.12999, doi: [10.48550/arXiv.2601.12999](https://doi.org/10.48550/arXiv.2601.12999)
- Özel, F., Psaltis, D., Narayan, R., & Santos Villarreal, A. 2012, *apj*, 757, 55, doi: [10.1088/0004-637X/757/1/55](https://doi.org/10.1088/0004-637X/757/1/55)
- Paparo, M., Szeidl, B., & Mahdy, H. A. 1988, *apss*, 149, 73, doi: [10.1007/BF00640467](https://doi.org/10.1007/BF00640467)
- Pápics, P. I. 2012, *Astronomische Nachrichten*, 333, 1053, doi: [10.1002/asna.201211809](https://doi.org/10.1002/asna.201211809)
- Paxton, B., Bildsten, L., Dotter, A., et al. 2011, *apjs*, 192, 3, doi: [10.1088/0067-0049/192/1/3](https://doi.org/10.1088/0067-0049/192/1/3)
- Paxton, B., Cantiello, M., Arras, P., et al. 2013, *apjs*, 208, 4, doi: [10.1088/0067-0049/208/1/4](https://doi.org/10.1088/0067-0049/208/1/4)
- Paxton, B., Marchant, P., Schwab, J., et al. 2015, *apjs*, 220, 15, doi: [10.1088/0067-0049/220/1/15](https://doi.org/10.1088/0067-0049/220/1/15)
- Paxton, B., Schwab, J., Bauer, E. B., et al. 2018, *apjs*, 234, 34, doi: [10.3847/1538-4365/aaa5a8](https://doi.org/10.3847/1538-4365/aaa5a8)
- Ricker, G. R., Winn, J. N., Vanderspek, R., et al. 2015, *Journal of Astronomical Telescopes, Instruments, and Systems*, 1, 014003, doi: [10.1117/1.JATIS.1.1.014003](https://doi.org/10.1117/1.JATIS.1.1.014003)
- Rogers, F. J., & Nayfonov, A. 2002, *ApJ*, 576, 1064, doi: [10.1086/341894](https://doi.org/10.1086/341894)
- Saio, H. 1981, *ApJ*, 244, 299, doi: [10.1086/158708](https://doi.org/10.1086/158708)
- Samolyk, G. 2010, *jaavso*, 38, 12
- . 2011, *jaavso*, 39, 23
- . 2012, *jaavso*, 40, 923
- . 2013, *jaavso*, 41, 85
- Wils, P., Ayiomamitis, A., Vanleenhove, M., et al. 2013, *Information Bulletin on Variable Stars*, 6049, 1
- Yi, T., Gu, W.-M., Zhang, Z.-X., et al. 2022, *Nature Astronomy*, 6, 1203, doi: [10.1038/s41550-022-01766-0](https://doi.org/10.1038/s41550-022-01766-0)